Mislinski_MoTrPAC_Redox_v11

Jack Mislinski[1], Andrew W. Subudhi[1], Robert A. Jacobs[1]

May 2026 — DRAFT v11

[1] Department of Human Physiology & Nutrition, University of Colorado Colorado Springs, Colorado Springs, CO, USA

Corresponding author: Jack Mislinski, jackmis610@gmail.com

Advisors: Dr. Andrew W. Subudhi, Dr. Robert A. Jacobs — University of Colorado Colorado Springs

Target journal: *Redox Biology* | **Status:** DRAFT v11 — internal review only

---

Abstract

Endurance exercise training reliably expands mitochondrial electron transport system (ETS) capacity across tissues, but whether NADPH-dependent redox buffering systems scale proportionally — and whether that relationship differs between sexes — has not been systematically characterized. The Vandiver–Neufer thermodynamic framework predicts that improved ETS coupling efficiency should reduce per-unit ROS generation, yielding sub-linear buffering scaling relative to ETS expansion. We tested this prediction using an 85-gene set organized by thermodynamic function, applied to the MoTrPAC rat endurance training dataset (19 tissues, 5 omic layers, 4 training time points, both sexes; 42,770 observations). After 8 weeks of training, transcriptional investment in redox buffering scaled sub-linearly with ETS expansion in both sexes. The female result was fully robust: $\beta = 0.31$ [0.10, 0.52] ($R^2 = 0.42$, $p(\beta < 1) = 2.8 \times 10^{-6}$, n = 16 tissues), stable under all single-tissue exclusions. For males, we report a conservative estimate excluding two influential tissues (BAT, BLOOD) as the headline value: $\beta = 0.55$ [0.28, 0.82] ($R^2 = 0.57$, $p = 0.0017$, n = 16); the full-model estimate is $\beta = 0.65$ (Table 1). The male result was directionally consistent across sensitivity scenarios but

sensitive to BAT inclusion, where a multi-feature mapping artifact inflates Cook's distance (D = 16.7). Critically, the sub-linear scaling pattern replicated in an independent omic layer: at the protein level (PROT, 7 tissues with 8w proteomics — none of which are BAT or BLOOD), males showed $\beta = 0.43$ [0.19, 0.66] ($R^2 = 0.81$, $p(\beta < 1) = 7.6 \times 10^{-4}$) and females $\beta = 0.22$ [0.04, 0.39] ($R^2 = 0.67$, $p(\beta < 1) = 4.2 \times 10^{-5}$), with the same sex-dimorphic pattern despite per-feature effect sizes being individually modest (median $|\log_2 FC| \approx 0.06$). The male protein result holds under leave-one-out ($\beta = 0.43$, $p = 0.006$ minus SKM-GN, $n = 6$); the female protein result reduces to a directional trend under leave-one-out ($\beta = 0.28$, $p = 0.058$, $n = 6$), reflecting the limited power of $n = 7$. Gene-level analysis revealed internal dissociation within the buffering circuit: front-line scavengers GPx4 and Txn2 tracked ETS near-perfectly ($r > 0.97$), thioredoxin reductase 2 (Txnrd2) scaled positively ($r = +0.72$, $p = 0.001$), while NNT showed a non-significant negative cross-tissue trend ($r = -0.40$, $p = 0.11$) — a pattern interpretable only through the thermodynamic circuit structure. Sex differences in scaling mapped onto distinct quality control programs: males coordinated ETS with damage-sensing mtUPR ($r = 0.80$) and mitophagy ($r = 0.74$); females coordinated through energy-sensing AMPK ($r = 0.68$). These transcript-level findings indicate that trained tissues show a sex-dimorphic mismatch between transcriptional investment in oxidative capacity and redox buffering, with the degree and tissue-specific drivers differing by sex.

Keywords: mitochondria · redox buffering · NNT · glutathione · electron transport system · exercise training · sex dimorphism · MoTrPAC · AMPK · thermodynamic framework

---

1. Introduction

Endurance exercise training is the most potent physiological stimulus for expanding mitochondrial oxidative capacity in mammalian tissues. Decades of research have characterized the transcriptional, proteomic, and functional signatures of this adaptation — upregulation of electron transport system (ETS) subunits, enhanced citrate synthase activity, increased cristae density, and improved coupling efficiency — in skeletal muscle and, more recently, across a broader tissue repertoire [1,2]. Yet the

ETS represents only one arm of the mitochondrial functional unit. Embedded within the same inner membrane and intimately coupled to the proton-motive force (Δp) is a network of NADPH-dependent redox buffering systems — glutathione peroxidases, glutathione reductase and biosynthetic enzymes [22], the thioredoxin reductase–thioredoxin–peroxiredoxin axis, and the nicotinamide nucleotide transhydrogenase (NNT) that regenerates mitochondrial NADPH from NADH — collectively neutralizing reactive oxygen species (ROS) and maintaining proteome redox tone across an estimated 17,000 redox-sensitive cysteine residues [3,28]. Whether these two functional arms scale proportionally with training, and whether that relationship differs between sexes, has never been systematically characterized.

The thermodynamic framework developed by Vandiver & Neufer [4] provides a specific, mechanistically grounded basis for a testable prediction. ΔG_{redox} drives ΔG_{pmf}, which drives both ATP synthesis and, via NNT, NADPH regeneration. The glutathione and thioredoxin buffering systems are thermodynamically downstream of NNT — their reducing power supplied by the NADPH pool NNT sustains. If training improves ETS coupling efficiency — reducing per-complex electron leak — then ROS generation per unit capacity decreases, reducing per-cycle NADPH demand [27]. This framework therefore generates a testable prediction: one would expect sub-linear buffering scaling — a regression slope of buffering on ETS significantly less than one, with the NADPH supply arm (NNT) nominally recalibrating downward while front-line scavengers (GPx4, Txn2) and thioredoxin reductase (Txnrd2) continue tracking ETS expansion [29]. This prediction is distinct from the mitohormesis framework [5], which posits that ROS function as signaling molecules driving beneficial adaptations; the Neufer framework specifically addresses the stoichiometric relationship between oxidative capacity and buffering investment at steady state.

The MoTrPAC rat endurance training dataset (19 tissues, 9 assay types, 4 time points, both sexes) [1,2] provides the multi-tissue resource to test this prediction. We constructed an 85-gene set organized by thermodynamic function (Figure 1) and applied it to 42,770 observations from the full

MoTrPAC resource to ask whether training is associated with proportional expansion of both ETS capacity and redox protection — and whether males and females answer differently.

---

2. Methods

2.1. Data source

Publicly available data from the MoTrPAC rat endurance training study (*Nature* 2024 [1]; *Cell Metabolism* 2024 [2]) accessed via the MotrpacRatTraining6moData R package (v2.0.0, Bioconductor). Fischer 344 rats, ~6–8 per group per sex per time point, 19 tissues. The full MoTrPAC resource includes 9 assay types; the present analysis uses 5 omic layers — transcriptomics (TRNSCRPT), proteomics (PROT), phosphoproteomics (PHOSPHO), acetylproteomics (ACETYL), and ubiquitylproteomics (UBIQ); metabolomics, immunoassays, ATAC-seq, and methylation are not used here. Pre-computed differential statistics used throughout; no raw data were reprocessed. Analyses conducted in R v4.5.2.

2.2. Gene set construction

85 genes in 15 functional categories based on Vandiver & Neufer [4], defined before examining MoTrPAC results. 84 genes mapped to MoTrPAC feature identifiers; Prodh absent. Full gene set in Supplementary Table 1 (`data/supplementary_table1_gene_set.csv`).

2.3. ETS and buffering indices

ETS index: mean $\log_2$FC of 32 ETS + ATP synthase genes (CI: Ndufs1, Ndufs2, Ndufs3, Ndufs7, Ndufs8, Ndufv1, Ndufv2, Ndufa9, Ndufa10, Ndufb8; CIII: Uqcrc1, Uqcrc2, Uqcrfs1, Uqcrb, Cyc1; CIV: Cox4i1, Cox5a, Cox5b, Cox6a1, Cox6b1, Cox7a2; cytochrome c: Cycs; ATP synthase: Atp5f1a, Atp5f1b, Atp5f1c, Atp5f1d, Atp5f1e, Atp5pb, Atp5mc1, Atp5mc2, Atp5mc3, Atp5po). Buffering index: mean $\log_2$FC of 14 genes (GSH system: Gpx1, Gpx4, Gsr, Gclc, Gclm, Gss, Glrx2; TRX system: Txn2, Txnrd2, Prdx3, Prdx5; NNT; SOD: Sod1, Sod2).

2.4. Regression and sensitivity analyses

OLS regression, buffering ~ ETS. One-sided t-test H_0: $\beta = 1$ ($p(\beta < 1)$). Cook's distance with threshold 4/n. Leave-one-tissue-out and pairwise exclusion scenarios for both sexes (Table 1). Male Cook's D > threshold: BAT (D = 16.7), BLOOD (D = 2.54). Female Cook's D > threshold: ADRNL (D = 11.3), BAT (D = 0.35).

2.5. Gene-by-gene correlations

Pairwise Pearson r between all 32 ETS and 14 buffering genes (8w $\log_2$FC, males) with and without BAT. Txnrd2 and NNT vs. ETS index compared in both sexes with and without BAT.

2.6. Permutation test

1,000 random gene sets (32 + 14 split) from 11,167 complete-data genes, BAT excluded. Empirical p for observed R^2 (curated $R^2 = 0.855$).

2.7. Protein-level regression

The transcript-level ETS index and buffering index (Section 2.3) were computed analogously at the protein level using MoTrPAC PROT data at 8 weeks. Seven tissues have proteomics at this time point (CORTEX, HEART, KIDNEY, LIVER, LUNG, SKM-GN, WAT-SC); BAT and BLOOD have no PROT data at any time point. Per tissue × sex, the protein ETS index is the mean $\log_2$FC across 33–37 PROT features matching the gene set in Section 2.3, and the protein buffering index is the mean $\log_2$FC across the 14 buffering proteins. The 33–37 ETS feature range reflects multiple PROT features per gene for some proteins (different RefSeq accessions/peptides per gene); the underlying gene set is identical to the transcript ETS index and the per-tissue feature count varies modestly with proteomic coverage. PROT features include only base-protein measurements (PHOSPHO, ACETYL, and UBIQ PTM-site features were excluded). OLS regression buffering ~ ETS at the protein level was performed by sex, with the same one-sided t-test against H_0: $\beta = 1$ used for the transcript regression. Pooled feature-level effect-size summaries (median $|\log_2$FC$|$, fraction with positive $\log_2$FC, two-sided binomial sign test) were computed across all features in each arm × sex.

2.8. Human data

MoTrPAC PASS1A human acute exercise dataset [9,10]. Feature-level log_2FC and adj_p from Keshishian et al. [9] Supplementary Table 3 ("Comparisonto_Reitzner" sheet, 13,059 genes). All values verified from downloaded files (`data/human/705181_target_genes.csv`).

2.9. Quality control gene set

A 72-gene set in 16 functional categories was used to characterize sex-dimorphic mitochondrial quality control programs (Section 3.7). Categories were organized across three rings and a bridge: Ring 1 (lactate–mitochondria axis: MPC, PDH complex, MCT transporters, HCAR1); Ring 2 (dynamics: fission [Fis1, Mff, Dnm1l], fusion [Mfn1, Mfn2, Opa1], mitophagy [Pink1, Prkn, Bnip3], biogenesis [Ppargc1a and PGC-1α target genes [23]]); Ring 3 (quality control signaling: mtUPR [Hspd1, Hspe1, ClpP], calcium handling [Vdac1–3, Mcu], AMPK axis [Prkaa1, Prkaa2, Ulk1]); bridge (ROS signaling: Nfe2l2, Keap1, Hmox1, Nqo1, Txnip). All 72 genes mapped to MoTrPAC feature identifiers. Cross-tissue Pearson r was computed between each category mean log_2FC and the ETS index at 8 weeks, separately for each sex.

2.10. Software

R v4.5.2 with MotrpacRatTraining6moData v2.0.0, MotrpacRatTraining6mo, tidyverse, ggplot2, patchwork, ggrepel, ComplexHeatmap. Python 3 with reportlab for table PDFs. All adj_p values are MoTrPAC consortium FDR (Benjamini–Hochberg).

---

3. Results

3.1. A curated thermodynamic gene set captures the Neufer redox circuit

We constructed an 85-gene set in 15 functional categories corresponding to nodes in the Neufer circuit (Supplementary Table 1; Figure 1): ETS electron carriers (Complexes I, III, IV; cytochrome c), ATP synthase, NNT, glutathione system (GPx1, GPx4, GSR, GCLC, GCLM, GSS, Glrx2), thioredoxin system (Txn2, Txnrd2, Prdx3, Prdx5), superoxide dismutases, and Q-pool feeders, PDH complex, beta-oxidation, and shuttle enzymes. Of 85 genes, 84 mapped to MoTrPAC feature identifiers (Prodh absent

from annotation). Querying 37 differential abundance tables yielded 42,770 observations across transcript, protein, phosphoprotein, acetylprotein, and ubiquitylprotein assays in 19 tissues at 4 time points in both sexes.

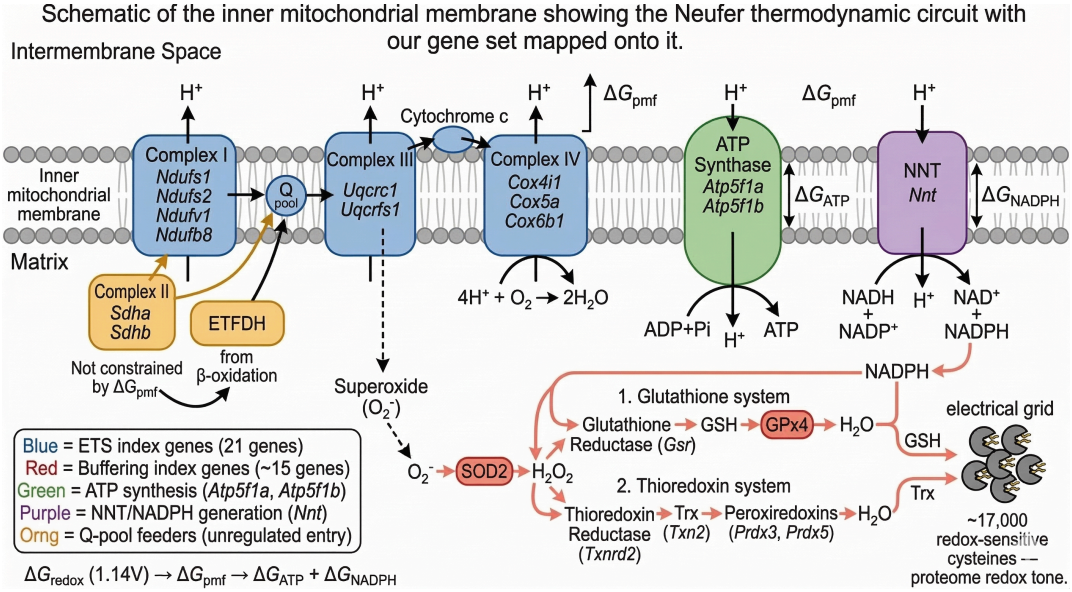

Vandiver–Neufer thermodynamic framework with curated gene set mapped onto the mitochondrial inner membrane. Blue: ETS index genes (Complexes I, III, IV, cytochrome c, ATP synthase). Red: redox buffering genes. Purple: NNT (ΔG_{pmf} → NADPH). Orange: Q-pool feeder enzymes. The thermodynamic cascade: $\Delta G_{redox} \rightarrow \Delta G_{pmf} \rightarrow \Delta G_{ATP} + \Delta G_{NADPH}$.

3.2. Trained animals exhibit sub-linear redox buffering scaling in both sexes

We computed tissue-level ETS indices (mean $\log_2$FC across 32 ETS + ATP synthase genes) and buffering indices (mean $\log_2$FC across 14 GSH/TRX/NNT/SOD genes) at 8 weeks versus sedentary baseline (Figure 2). At baseline, cross-tissue ETS–buffering correlation was weak ($R^2 = 0.20$ males, 0.18 females). Following 8 weeks of training, tissues showed sub-linear scaling in both sexes (buffering < ETS expansion).

Males: Cook's distance analysis identified BAT (D = 16.7) as massively influential via a multi-feature mapping artifact (negative ETS mean despite 22 individually significant genes), and BLOOD (D = 2.54) as the highest-leverage legitimate outlier. All five sensitivity scenarios show sub-linear slope estimates (Table 1); the exception is the BAT-only exclusion (β = 1.22, p = 0.945), confirming this single point drives the full-model male estimate. The conservative estimate excluding both (β = 0.55 [0.28, 0.82], $R^2 = 0.57$, p = 0.0017, n = 16) confirms that sub-linear scaling is present

and significant when both artifacts are removed. Leave-one-out analysis shows male sub-linearity is lost when BAT alone is excluded ($p = 0.945$) but maintained for every other single-tissue exclusion.

Females: Adrenal tissue emerged as the dominant influential point (Cook's $D = 11.3$), with BAT the second ($D = 0.35$). In contrast to males, female sub-linearity is fully robust: all 18 leave-one-out p-values < 0.05, regardless of which tissue is excluded. The conservative estimate excluding both BAT and ADRNL ($\beta = 0.31$ [0.10, 0.52], $R^2 = 0.42$, $p = 2.8 \times 10^{-6}$, $n = 16$) is directionally consistent with the full-model estimate ($\beta = 0.14$, $R^2 = 0.32$, $p = 6.5 \times 10^{-12}$), noting that excluding the high-leverage ADRNL (which has a strongly positive ETS index paired with a strongly negative buffering index) shifts the slope upward from 0.14 to 0.31 — both are substantially sub-linear. The female sub-linearity is the more statistically robust sex-specific finding.

Table 1. Sensitivity analysis of the ETS→buffering regression slope across tissue-exclusion scenarios (8-week TRNSCRPT). ★ = recommended primary estimate. BAT excluded from conservative male estimate due to multi-feature mapping artifact (Cook's $D = 16.7$); ADRNL excluded from conservative female estimate as dominant influential point (Cook's $D = 11.3$). See Supplementary Figure 4 for full Cook's distance and leave-one-out diagnostics.

Scenario	n	β	95% CI	R^2	p(β < 1)
MALES					
All tissues	18	0.65	[0.43, 0.87]	0.72	0.0018
Minus BAT	17	1.22	[0.94, 1.50]	0.86	0.945
Minus BLOOD	17	0.45	[0.36, 0.53]	0.90	1.6×10^{-10}
Minus BAT + BLOOD ★	16	0.55	[0.28, 0.82]	0.57	0.0017
Minus top-3	15	0.69	[0.38, 1.00]	0.65	0.023
FEMALES					
All tissues	18	0.14	[0.03, 0.25]	0.32	6.5×10^{-12}
Minus BAT	17	0.11	[0.01, 0.21]	0.28	2.1×10^{-12}
Minus ADRNL	17	0.37	[0.21, 0.54]	0.62	2.9×10^{-7}
Minus BAT + ADRNL ★	16	0.31	[0.10, 0.52]	0.42	2.8×10^{-6}
Minus top-3	15	0.31	[0.15, 0.47]	0.57	2.6×10^{-7}

(Top-3 for males: BAT + BLOOD + SKM-GN; for females: ADRNL + BAT + SPLEEN)

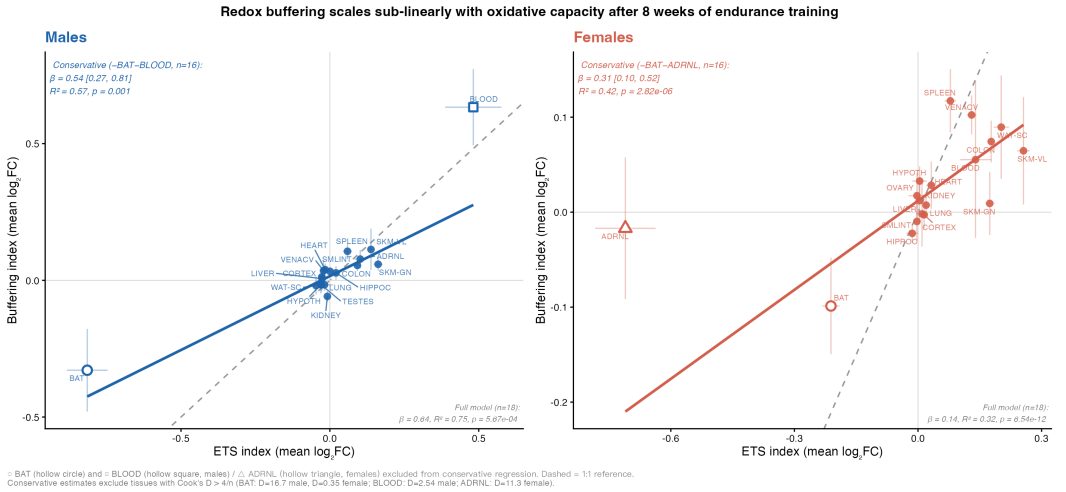

○ BAT (hollow circle) and □ BLOOD (hollow square, males) / △ ADRNL (hollow triangle, females) excluded from conservative regression. Dashed = 1:1 reference.
Conservative estimates exclude tissues with Cook's D > 4/n (BAT: D=16.7 male, D=0.35 female; BLOOD: D=2.54 male; ADRNL: D=11.3 female).

Sex-dimorphic association of redox buffering with oxidative capacity in trained animals (8-week endurance training, TRNSCRPT). Each point = one tissue; x-axis = ETS index (mean $\log_2$FC of 32 ETS + ATP synthase genes vs. sedentary); y-axis = buffering index (mean $\log_2$FC of 14 GSH/TRX/NNT/SOD genes). Error bars: ±1 SE across genes. Dashed line = 1:1 proportional reference. Regression line shows conservative estimate in each panel. **Left (males):** Conservative (–BAT–BLOOD, n=16): β = 0.55 [0.28, 0.82], R^2 = 0.57, p = 0.0017. BAT = hollow circle (○); BLOOD = hollow square (□) — both excluded from conservative regression. Full-model statistics annotated in lower right. **Right (females):** Conservative (–BAT–ADRNL, n=16): β = 0.31 [0.10, 0.52], R^2 = 0.42, p = 2.8×10^{-6}. BAT = hollow circle (○); ADRNL = hollow triangle (△) — both excluded from conservative regression.

3.3. Sub-linear scaling replicates at the protein level (independent omic layer)

To address whether the transcript-level result reflects post-transcriptional regulation rather than a real change in functional protein content, we repeated the regression at the protein level using MoTrPAC PROT data at 8 weeks (Figure 3). Seven tissues have proteomics at this time point — CORTEX, HEART, KIDNEY, LIVER, LUNG, SKM-GN, and WAT-SC — and importantly, neither BAT nor BLOOD (the two influential tissues in the male transcript regression) is among them, so the protein analysis is *de facto* a conservative sensitivity test of the male result. ETS index: mean $\log_2$FC across 33–37 PROT features per tissue; buffering index: 14 PROT features per tissue (matched to the gene set in Section 2.3, with PTM-site features excluded).

Per-feature effect sizes are individually modest at the protein level — median $|\log_2 FC| \approx 0.06$ for ETS and ≈ 0.06 for buffering proteins, with most individual proteins not surviving FDR correction at the per-tissue × per-protein level — but the pooled directional signal is robust: across all 245 ETS protein observations in males, 57.6% show positive $\log_2$FC (sign-test $p = 0.021$); for the 98 buffering protein observations, 66.3% are positive ($p = 0.0016$). In females, the pooled signal is stronger still (ETS frac-positive = 0.75, buffering = 0.63). These pooled effect sizes are too small to register as individual-protein differential expression but large enough in aggregate to reproduce the cross-tissue scaling pattern.

The protein-level regression mirrors the transcript result in both magnitude and direction. Males: $\beta = 0.43$ [0.19, 0.66], $R^2 = 0.81$, $p(\beta < 1) = 7.6 \times 10^{-4}$ ($n = 7$). Females: $\beta = 0.22$ [0.04, 0.39], $R^2 = 0.67$, $p(\beta < 1) = 4.2 \times 10^{-5}$ ($n = 7$). The male protein slope (0.43) is consistent with — and slightly below — both transcript estimates (full-model 0.65, conservative 0.55), and the female protein slope (0.22) is within overlapping confidence intervals of the female transcript conservative estimate (0.31). Both sex-specific 95% CIs exclude the proportional value of 1 in the protein analysis, the protein R^2 is *higher* than the transcript R^2 in both sexes (0.81 vs 0.57 male, 0.67 vs 0.42 female), and the same female-stronger-than-male pattern of sub-linearity is preserved. Removing SKM-GN (the highest-leverage protein-level point)

preserves significance in males (β = 0.43, p(β < 1) = 0.006, n = 6) but reduces the female result to a directional trend (β = 0.28, p = 0.058, n = 6), reflecting the limited statistical power of n = 6.

Importantly, the high R^2 of the protein regression cannot be reduced to averaging artefact: tissue-level means could in principle smooth uncorrelated noise into apparent structure, but it is the *cross-tissue covariance* between the ETS and buffering means — not the means individually — that the regression measures. The same averaging applied to randomly drawn ETS- and buffering-sized gene sets at the transcript level recovers near-zero R^2 on average (Section 3.4 permutation test, null mean β = 0.21, SD = 1.21), and the per-feature pooled sign-test (p = 0.0016 for buffering proteins in males) confirms a directional signal at the level of individual proteins, not just tissue means.

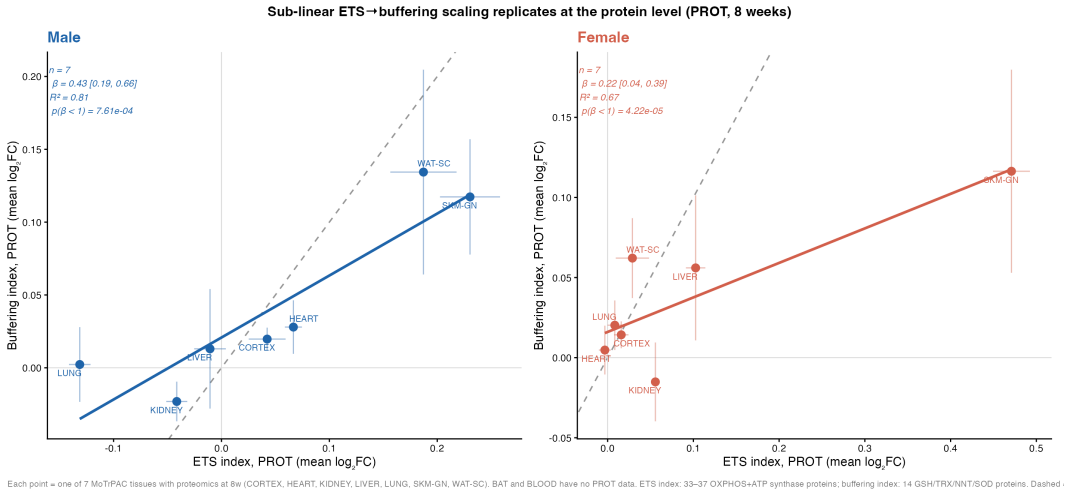

Each point = one of 7 MoTrPAC tissues with proteomics at 8w (CORTEX, HEART, KIDNEY, LIVER, LUNG, SKM-GN, WAT-SC). BAT and BLOOD have no PROT data. ETS index: 33–37 OXPHOS+ATP synthase proteins; buffering index: 14 GSH/TRX/NNT/SOD proteins. Dashed

Protein-level replication of the ETS→buffering regression (8 weeks of training, MoTrPAC PROT data, 7 tissues per sex). Each point = one tissue. ETS index: mean $\log_2$FC of 33–37 OXPHOS/ATP synthase proteins. Buffering index: mean $\log_2$FC of 14 GSH/TRX/NNT/SOD proteins. Dashed line: 1:1 reference. Annotated: regression slope, 95% CI, R^2, and p(β < 1) per sex. Both BAT and BLOOD — the two influential tissues in the male transcript regression — are absent from this analysis as MoTrPAC has no proteomics in those tissues, providing an independent sensitivity test.

3.4. Curated framework outperforms compartment-based annotation

A permutation test with 1,000 random gene sets (BAT excluded, 11,167-gene universe) confirmed framework specificity: curated R^2 = 0.855 exceeded 99.4% of random permutations (p = 0.006). Sub-linear scaling between arbitrary gene pairs is the default (null mean β = 0.21, SD = 1.21); the framework's value is its tight cross-tissue coupling (high R^2). MitoCarta 3.0 comparison (Supplementary Figure 2) confirmed: OXPHOS vs. ROS

defense yielded β = 1.12, R^2 = 0.33, no sub-linearity (p = 0.62). The localization-based approach includes cytoplasmic antioxidants and non-ΔG_{pmf}-coupled enzymes that dilute the thermodynamic signal.

3.5. Tissue response profiles

Individual tissues varied in their ETS–buffering response pattern (Supplementary Figure 1). SKM-GN showed the largest male buffering deficit (ETS $\log_2$FC = 0.175, buffering = 0.034, ratio = 0.35), while BLOOD and SKM-VL showed near-proportional scaling. BAT and ADRNL, the two tissues identified as influential outliers (Section 3.2), both showed negative indices on one or both axes; BAT operates under distinct thermodynamic constraints due to UCP1-mediated proton leak and is treated as a sensitivity case throughout. Most brain, visceral, and immune tissues showed minimal response on either axis.

3.6. Front-line scavengers and Txnrd2 scale proportionally; NNT shows a directional trend

Pairwise Pearson correlations between all 32 ETS genes and 14 buffering genes (8-week $\log_2$FC, males, BAT excluded; Figure 4) revealed striking internal dissociation. GPx4 and Txn2 — front-line scavengers structurally co-localized with ETS complexes — tracked ETS near-perfectly (Atp5f1b–Txn2: r = 0.980; Atp5f1b–GPx4: r = 0.979; Cox6a1–GPx4: r = 0.978). These enzymes directly scavenge H_2O_2 at the site of generation; their proportional scaling with ETS is consistent with maintained membrane-level peroxide defense.

NNT showed a predominantly negative cross-tissue trend after BAT exclusion: 20 of 32 ETS genes exhibited negative correlations with NNT $\log_2$FC (BAT excluded, males, 8w). The correlation with the composite ETS index was r = −0.40 (p = 0.11, n = 17 tissues) — directionally consistent with the Vandiver–Neufer prediction but not achieving statistical significance. When BAT is included, the correlation is r = −0.87 ($p < 0.001$, n = 18), driven in part by BAT's anomalous ETS profile. Given BAT's established methodological artifact, the BAT-excluded result (r = −0.40, p = 0.11) should be interpreted as a non-significant negative trend requiring confirmation with larger tissue panels or protein-level data.

Txnrd2 — the primary NADPH consumer in the thioredoxin circuit [29] — scaled positively with ETS: r = +0.72 (p = 0.001, BAT excluded). This dissociation between NNT (nominal negative trend) and Txnrd2 (significant positive scaling) indicates that the thioredoxin circuit arm maintains stoichiometric capacity with ETS expansion, even if upstream NADPH supply nominally trends downward.

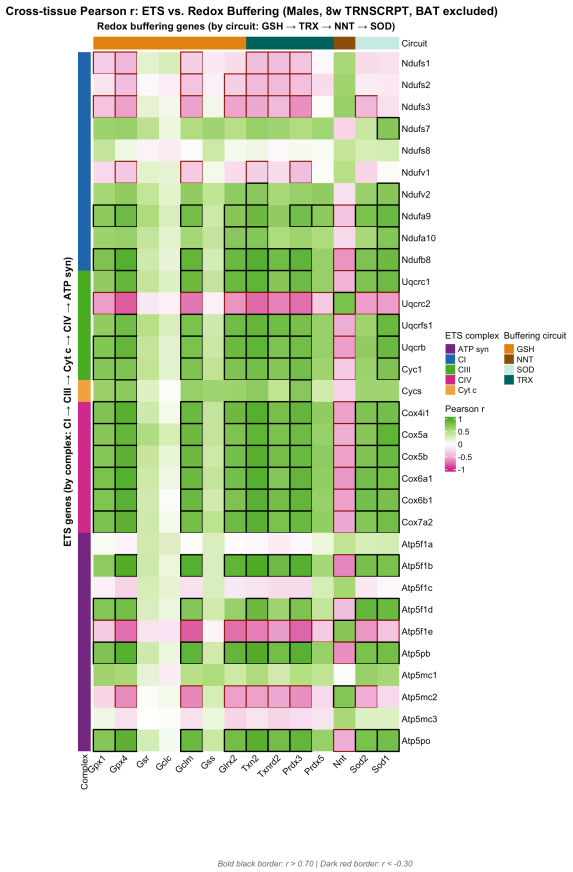

Gene-by-gene Pearson correlation heatmap (males, BAT excluded, 17 tissues). Rows: 32 ETS genes annotated by complex (left sidebar). Columns: 14 buffering genes. Color: cross-tissue Pearson r of 8-week $\log_2$FC. Bold black borders: r > 0.70. Dark red borders: r < –0.30.

3.7. Sex-dimorphic quality control programs

A parallel 72-gene set covering mitochondrial dynamics and signaling (Figure 5) revealed different coordination architectures by sex. **Males:** damage-sensing programs scaled with ETS — mtUPR (r = 0.80, p = 6.1 × 10^{-5}), mitophagy (r = 0.74, p = 4.3 × 10^{-4}), calcium handling (r = 0.80). **Females:** energy-sensing AMPK (r = 0.68, p = 0.002) dominated, while

mtUPR (r = 0.32) and mitophagy (r = 0.21) were non-significant. Biogenesis showed no sex dimorphism (r ≈ 0.60 both). Fission, fusion, and DRP1 phosphoproteomics showed near-zero ETS coupling in both sexes (312 observations, zero significant after FDR correction).

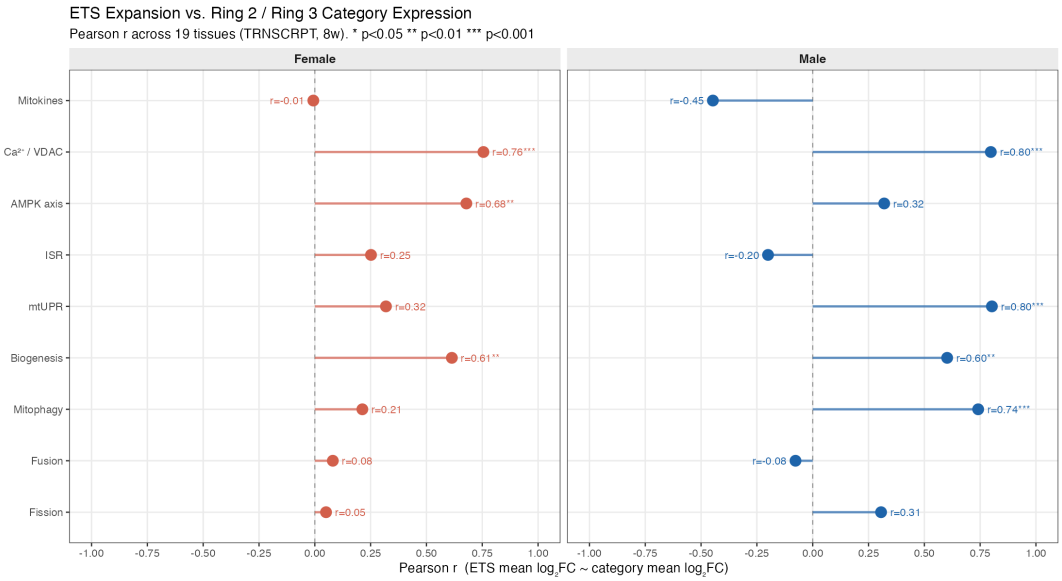

Sex-dimorphic coupling of mitochondrial quality control programs to ETS expansion (cross-tissue Pearson r, 8w TRNSCRPT). Males (blue): damage-sensing programs — mtUPR (r = 0.80***), mitophagy (r = 0.74***) — scale tightly. Females (red): energy-sensing AMPK (r = 0.68**) dominates. Biogenesis (r ≈ 0.60**) shows no sex dimorphism. * p < 0.05; ** p < 0.01; *** p < 0.001.

3.8. Temporal dynamics: non-monotonic male trajectory, consistent female sub-linearity

The ETS–buffering association showed divergent temporal trajectories by sex (Figure 6). The male trajectory was non-monotonic (BAT included throughout; interpret accordingly): at 1 week, β = 0.25 (R^2 = 0.36); at 2 weeks, β = 0.71 (R^2 = 0.42, p = 0.088) — the only time point where sub-linearity was not statistically significant, consistent with a transient window of near-proportional defensive upregulation; by 4 weeks, β = 0.38 (R^2 = 0.39); and by 8 weeks β = 0.65 (R^2 = 0.72), as chronic adaptations mature. Females showed consistently sub-linear slopes throughout (β = 0.12–0.31, all $p < 10^{-6}$), with no transient proportional window at any time point — the sex divergence in ETS–buffering scaling is present from the earliest measured response.

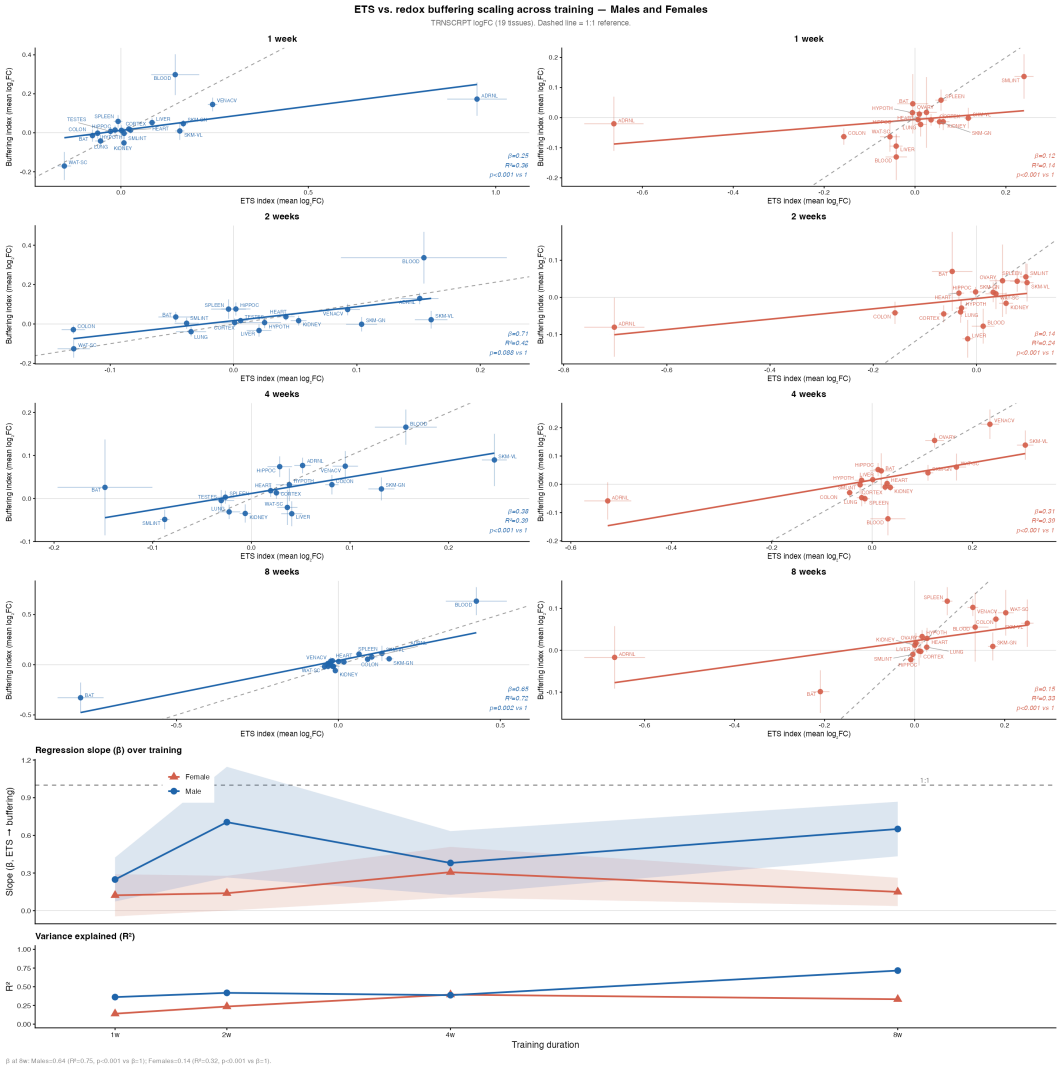

Temporal evolution of ETS–buffering association in both sexes (BAT included). Top panels: cross-tissue scatter at 1, 2, 4, and 8 weeks for males (blue) and females (red). Bottom: slope (β, 95% CI) and R^2 trajectories by sex. Males show a non-monotonic pattern with a transient near-proportional window at 2 weeks (β = 0.71, p = 0.088) followed by progressive sub-linear recalibration. Females show consistently sub-linear slopes throughout (β = 0.12–0.31, all $p < 10^{-6}$).

3.9. SKM-GN: largest buffering deficit with significant transcript–protein concordance

Gastrocnemius showed the largest male buffering deficit (ratio = 0.35) and the only significant *per-tissue* ETS transcript–protein Pearson concordance among the 7 tissues with proteomics (r = 0.577, p = 0.002 across the 32 ETS gene pairs within SKM-GN — a different analysis from the cross-tissue index regression in Section 3.3), confirming that transcriptional ETS upregulation is translated to the proteome in the primary locomotor

muscle. mtUPR was the top quality control correlate in SKM-GN males (r = 0.80), positioning this tissue as operating near the limits of mitochondrial protein homeostasis during remodeling.

3.10. Human acute exercise data show independent regulation of ETS and buffering programs

To assess cross-species relevance, we queried the MoTrPAC PASS1A human acute exercise dataset [9,10] (skeletal muscle transcriptomics, 13,059 genes). This comparison involves a different species, experimental design (single acute bout vs. 8-week chronic training), and tissue scope (skeletal muscle only vs. 19 tissues), so convergence is evaluated at the level of regulatory independence rather than matching effect sizes. ETS genes (ATP5F1B, NDUFV1, COX4I1, CYCS) were elevated selectively at 24h after endurance exercise, while buffering genes GCLM (adj_p = 1.3×10^{-6}), SOD2 (adj_p = 0.003), and GPX4 (adj_p = 0.038) were elevated at 3.5h after resistance exercise. NNT was non-significant in both modalities (adj_p = 0.28). The human SC-ION network identified distinct upstream regulators for each circuit — NFIC phosphorylation driving ETS gene transcription under endurance, FOXO3 phosphorylation driving GCLM/SOD2 under resistance — consistent with independent transcriptional programs for the two arms of the mitochondrial functional unit [6,7]. The forthcoming MoTrPAC chronic training dataset (PASS1B) will provide the definitive human analog of the rat 8-week data.

4. Discussion

The central finding is that investment in redox buffering scales sub-linearly with ETS expansion across tissues following endurance training — at *both* the transcript and protein levels — and that the degree of this mismatch differs by sex. The female result is the more robust: β = 0.31 at the transcript level (stable under all single-tissue exclusions) and β = 0.22 at the protein level, with both 95% CIs excluding 1. The male result is directionally consistent (β = 0.55 transcript conservative; β = 0.43 protein) and the protein replication is particularly informative because the seven tissues with proteomics do not include BAT or BLOOD — the two influential tissues responsible for the male transcript-level fragility. The protein analysis therefore functions as an independent sensitivity test, and

the male sub-linearity is preserved with $R^2 = 0.81$ and $p(\beta < 1) = 7.6 \times 10^{-4}$. The agreement of independent omic layers — and the concordance of the female-stronger-than-male pattern — substantially raises our confidence that the scaling result is biological rather than transcriptional regulatory noise. To our knowledge, this is the first empirical quantification of ETS–buffering proportionality across a full mammalian tissue repertoire.

The gene-by-gene analysis reveals informative sub-structure within the buffering circuit. Front-line scavengers GPx4 and Txn2 track ETS at $r > 0.97$ across tissues, indicating that trained tissues scale membrane-level peroxide defense in lock-step with oxidative capacity at the transcript level — not "approximately" but at near-perfect proportionality across the entire 17-tissue panel. This is the cleanest result in the dataset and is consistent with the thermodynamic prediction that terminal H_2O_2-scavenging capacity must keep pace with ETS expansion at sites of generation, even when overall buffering investment is sub-linear. NNT shows a negative cross-tissue trend after BAT exclusion ($r = -0.40$, $p = 0.11$). If this trend reflects a genuine biological pattern — which will require confirmation in larger panels or at the protein level — it would be consistent with reduced per-unit ROS production requiring less NADPH regeneration under improved coupling efficiency [27]. Txnrd2 scales positively with ETS ($r = +0.72$, $p = 0.001$), indicating that the thioredoxin circuit maintains stoichiometric transcript-level investment with ETS expansion even as the upstream NADPH supply nominally trends downward. This combination — proportional terminal defense with nominal upstream recalibration — is only interpretable through the thermodynamic circuit structure of the Neufer framework; MitoCarta's ROS category, which does not separate by thermodynamic position, yields $\beta = 1.12$, $R^2 = 0.33$ — no signal. The human acute exercise data (Section 3.10) are consistent at the level of regulatory independence: distinct upstream kinases drive ETS and buffering programs, though the different species and experimental design preclude direct quantitative comparison.

The sex divergence in quality control coupling is an observational association, not a demonstrated causal relationship, but it generates testable hypotheses. Males show coordinated ETS–mtUPR ($r = 0.80$) and ETS–mitophagy ($r = 0.74$) scaling, while females show ETS–AMPK coordination ($r = 0.68$) without equivalent damage-surveillance coupling. If

these associations reflect distinct homeostatic strategies, the molecular signatures of training stress would be expected to differ by sex — a hypothesis with potential relevance to sex-specific overtraining assessment [17].

Trained locomotor muscle (SKM-GN) showed the largest buffering deficit, protein-level ETS validation, and the strongest mtUPR coupling — consistent with operating near the limits of mitochondrial protein homeostasis during remodeling. Blood leukocytes showed near-proportional ETS–buffering scaling and the strongest single-gene signal in both rats (Atp5f1b, adj_p = 7.23×10^{-13}) and humans (ATP5F1B adj_p = 0.007), making leukocyte ETS transcripts a candidate for non-invasive monitoring. The transient near-proportional male window at 2 weeks may represent an early training phase of coordinated ETS–buffering induction before chronic divergence consolidates by 4–8 weeks.

4.1. Limitations

- The male transcript regression is sensitive to BAT (Cook's D = 16.7) and BLOOD (D = 2.54). The conservative transcript estimate ($\beta = 0.55$, $p = 0.0017$, $n = 16$) is significant, and the protein-level analysis (Section 3.3, $\beta = 0.43$, $p(\beta < 1) = 7.6 \times 10^{-4}$), which by data availability excludes both BAT and BLOOD, provides convergent evidence that the male scaling pattern is robust. The BAT multi-feature mapping artifact remains a transcript-level annotation issue and should be resolved with improved feature mapping for any future re-analysis.
- NNT's negative cross-tissue trend ($r = -0.40$) is directionally consistent with the NADPH economy recalibration hypothesis but does not reach statistical significance after BAT exclusion ($p = 0.11$). We report it as a non-significant trend, not an established finding.
- Aggregate sub-linear scaling is observed at both transcript and protein levels, but per-protein effect sizes are individually modest (median $|\log_2 FC| \approx 0.06$) and most individual proteins do not reach FDR significance at the per-tissue level. The pooled directional signal (sign-test $p = 0.002$ for buffering proteins) is what powers the regression. NNT's negative trend and Txnrd2's positive scaling are transcript-level observations and still require protein-level and activity-level confirmation in tissues where MoTrPAC has no PROT data.

- The rat-to-human gap, while mitigated by ≥149/150 gene ortholog conservation, does not account for species, sex hormone profile, or exercise intensity differences.
- Sub-linear scaling represents sub-linear transcriptional investment, not proven functional redox deficit. Direct measurement of NADPH/$NADP^+$ ratios, thioredoxin redox state, and ROS handling capacity in trained tissues is required.
- Gene-level quantification does not resolve isoform-level regulation; tissue-specific splicing effects may be masked.
- Statistical power derives from the 19-tissue cross-section (~6–8 rats per group), not from within-tissue replication. Correlation findings are tissue-level effects.

Data Availability

All rat multi-omic data used in this study are publicly available through the MoTrPAC Data Hub (motrpac-data.org) and the MotrpacRatTraining6moData R package (Bioconductor, v2.0.0). Human acute exercise data are available in the supplementary tables of Keshishian et al. (bioRxiv 10.64898/2026.03.04.705181). Analysis code, including all R and Python scripts used to generate figures and tables, is available at https://github.com/jackmis610/motrpac-redox. All statistical outputs are archived in the `data/` directory of the repository.

Author Contributions

J.M.: conceptualization, data curation, formal analysis, visualization, writing — original draft. A.W.S.: supervision, project administration, writing — review & editing. R.A.J.: supervision, conceptualization, writing — review & editing. All authors approved the final manuscript.

Conflict of Interest Statement

The authors declare no competing financial interests. This work received no commercial funding. J.M. is a graduate student; A.W.S. and R.A.J. are faculty advisors at the University of Colorado Colorado Springs. The

MoTrPAC dataset was generated by an independent consortium; the authors have no affiliation with MoTrPAC and conducted this as an independent secondary analysis.

References

1. MoTrPAC Study Group. Temporal dynamics of the multi-omic response to endurance exercise training across rat tissues. *Nature* 2024;629:174–183. doi:10.1038/s41586-023-06877-w
2. Amar D, et al. The mitochondrial multi-omic response to exercise training across rat tissues. *Cell Metabolism* 2024;36:1411–1429. doi:10.1016/j.cmet.2024.03.001
3. Xiao H, et al. A quantitative tissue-specific landscape of protein redox regulation during aging. *Cell* 2020;180:968–983.e24. doi:10.1016/j.cell.2020.02.012
4. Vandiver KJ, Neufer PD. Mitochondria: connecting oxygen to life. In: *On Oxygen*. Elsevier; 2025.
5. Ristow M, Schmeisser K. Mitohormesis: promoting health and lifespan by increased levels of reactive oxygen species (ROS). *Dose-Response* 2014;12:288–341. doi:10.2203/dose-response.13-035.Ristow
6. Murphy MP. How mitochondria produce reactive oxygen species. *Biochemical Journal* 2009;417:1–13. doi:10.1042/BJ20081386
7. Fisher-Wellman KH, Neufer PD. Linking mitochondrial bioenergetics to insulin resistance via redox biology. *Trends in Endocrinology & Metabolism* 2012;23:142–153. doi:10.1016/j.tem.2011.12.008
8. Fisher-Wellman KH, Lin CT, Ryan TE, Reese LR, Gilliam LAA, Cathey BL, Lark DS, Smith CD, Muoio DM, Neufer PD. Pyruvate dehydrogenase complex and nicotinamide nucleotide transhydrogenase constitute an energy-consuming redox circuit. *Biochemical Journal* 2015;467:271–280. doi:10.1042/BJ20141447
9. Keshishian H, et al. Integrative multi-omics analysis of the human skeletal muscle response to endurance or resistance exercise. *bioRxiv* 2026. doi:10.64898/2026.03.04.705181
10. MoTrPAC Study Group. Multi-omic, multi-tissue responses to acute exercise in sedentary adults. *bioRxiv* 2026. doi:10.64898/2026.02.27.702183
11. Egan B, Zierath JR. Exercise metabolism and the molecular regulation of skeletal muscle adaptation. *Cell Metabolism* 2013;17:162–184. doi:10.1016/j.cmet.2012.12.012
12. Peoples JN, et al. Effects of exercise training on mitochondrial function in cardiovascular diseases. *International Journal of Molecular Sciences* 2022;23:12559. doi:10.3390/ijms232012559
13. Tonkonogi M, et al. Mitochondrial function and antioxidative defence in human muscle: effects of endurance training and oxidative stress. *Journal of Physiology* 2002;528:379–388. doi:10.1111/j.1469-7793.2000.00379.x
14. Smith CD, et al. Flux through mitochondrial redox circuits linked to NNT and Nox4. *Journal of Biological Chemistry* 2020;295:16207–16216. doi:10.1074/jbc.RA120.013825
15. Ristow M, et al. Antioxidants prevent health-promoting effects of physical exercise in humans. *PNAS* 2009;106:8665–8670. doi:10.1073/pnas.0903485106

16. Anderson EJ, Lustig ME, Boyle KE, Woodlief TL, Kane DA, Lin CT, Price JW 3rd, Kang L, Rabinovitch PS, Szeto HH, Houmard JA, Cortright RN, Wasserman DH, Neufer PD. Mitochondrial H_2O_2 emission and cellular redox state link excess fat intake to insulin resistance in both rodents and humans. *Journal of Clinical Investigation* 2009;119:573–581. doi:10.1172/JCI37048
17. Mountjoy M, Sundgot-Borgen JK, Burke LM, Ackerman KE, Blauwet C, Constantini N, et al. IOC consensus statement on relative energy deficiency in sport (RED-S): 2018 update. *British Journal of Sports Medicine* 2018;52:687–697. doi:10.1136/bjsports-2018-099193
18. Steinberg GR, Hardie DG. New insights into activation and function of the AMPK. *Nature Reviews Molecular Cell Biology* 2023;24:255–272. doi:10.1038/s41580-022-00547-x
19. Lapuente-Brun E, Moreno-Loshuertos R, Acin-Perez R, Latorre-Pellicer A, Colas C, Balsa E, et al. Supercomplex assembly determines electron flux in the mitochondrial electron transport chain. *Science* 2013;340:1567–1570. doi:10.1126/science.1230381
20. Ventura-Clapier R, Moulin M, Piquereau J, Lemaire C, Mericskay M, Veksler V, Garnier A. Mitochondria: a central target for sex differences in pathologies. *Clinical Science* 2017;131:803–822. doi:10.1042/CS20160485
21. Hood DA, Memme JM, Oliveira AN, Triolo M. Maintenance of skeletal muscle mitochondria in health, exercise, and aging. *Annual Review of Physiology* 2019;81:19–41. doi:10.1146/annurev-physiol-020518-114310
22. Schafer FQ, Buettner GR. Redox environment of the cell as viewed through the redox state of the glutathione disulfide/glutathione couple. *Free Radical Biology and Medicine* 2001;30:1191–1212. doi:10.1016/S0891-5849(01)00480-4
23. Puigserver P, Wu Z, Park CW, Graves R, Wright M, Spiegelman BM. A cold-inducible coactivator of nuclear receptors linked to adaptive thermogenesis. *Cell* 1998;92:829–839. doi:10.1016/S0092-8674(00)81410-5
24. Ronchi JA, Figueira TR, Ravagnani FG, Oliveira HCF, Vercesi AE, Castilho RF. A spontaneous mutation in the nicotinamide nucleotide transhydrogenase gene of C57BL/6J mice results in mitochondrial redox abnormalities. *Free Radical Biology and Medicine* 2013;63:446–456. doi:10.1016/j.freeradbiomed.2013.05.049
25. Nickel AG, von Hardenberg A, Hohl M, Loffler JR, Kohlhaas M, Becker J, et al. Reversal of mitochondrial transhydrogenase causes oxidative stress in heart failure. *Cell Metabolism* 2015;22:472–484. doi:10.1016/j.cmet.2015.07.008
26. Sanford JA, Nogiec CD, Lindholm ME, et al. Molecular Transducers of Physical Activity Consortium (MoTrPAC): mapping the dynamic responses to exercise. *Cell* 2020;181:1464–1474. doi:10.1016/j.cell.2020.06.004
27. Brand MD. Mitochondrial generation of superoxide and hydrogen peroxide as the source of mitochondrial redox signaling. *Free Radical Biology and Medicine* 2016;100:14–31. doi:10.1016/j.freeradbiomed.2016.04.001
28. Go YM, Jones DP. Redox compartmentalization in eukaryotic cells. *Biochimica et Biophysica Acta* 2008;1780:1273–1290. doi:10.1016/j.bbagen.2008.01.011
29. Lu J, Holmgren A. The thioredoxin antioxidant system. *Free Radical Biology and Medicine* 2014;66:75–87. doi:10.1016/j.freeradbiomed.2013.07.036

Supplementary Material

Supplementary Figure 1. Tissue response profiles heatmap (8w, both sexes, TRNSCRPT). Four response archetypes: balanced expanders, ETS-deficit, suppressors, minimal responders.

Supplementary Figure 2. MitoCarta 3.0 vs. Neufer framework cross-tissue regression (males, 8w TRNSCRPT). Neufer: $\beta = 0.65$, $R^2 = 0.72$. MitoCarta OXPHOS vs. ROS: $\beta = 1.12$, $R^2 = 0.33$, no sub-linearity.

Supplementary Figure 3. Permutation test (BAT excluded). Null distributions of slope and R^2 from 1,000 random gene splits. Observed $R^2 = 0.855$ ($p = 0.006$).

Supplementary Figure 4. Cook's distance and leave-one-out slope stability (both sexes, 8w TRNSCRPT). **Males:** BAT ($D = 16.7$) massively influential; BLOOD ($D = 2.54$) moderately influential. Sub-linearity lost when BAT alone excluded ($p = 0.945$); maintained for all other single-tissue exclusions. **Females:** ADRNL ($D = 11.3$) dominant; BAT ($D = 0.35$) second. Sub-linearity maintained for ALL 18 single-tissue exclusions (all $p < 0.05$).

Supplementary Table 1. Complete 85-gene set with gene symbol, functional category, subcategory, Ensembl ID, Entrez ID, human ortholog, mapping status, and index membership. Available as `data/supplementary_table1_gene_set.csv`.